ELSEVIER

Lithos 45 (1998) 223–243

LITHOS

The alkaline–peralkaline granitic post-collisional Tin Zebane dyke swarm (Pan-African Tuareg shield, Algeria): prevalent mantle signature and late agpaitic differentiation

Zakia Hadj-Kaddour [a,1], Jean-Paul Liégeois [b,2], Daniel Demaiffe [a,*], Renaud Caby [c,3]

[a] *Géochimie Isotopique, CP 160 / 02, Université Libre de Bruxelles, 50 av F. Roosevelt, B-1050 Brussels, Belgium*
[b] *Dpt. de Géologie, Section de Géologie Isotopique, Musée Royal de l'Afrique Centrale, B-3080 Tervuren, Belgium*
[c] *Laboratoire de Tectonophysique, Université de Montpellier 2, F-34095 Montpellier, France*

Received 18 December 1997; accepted 30 June 1998

Abstract

The Tin Zebane dyke swarm was emplaced at the end of the Pan-African orogeny along a mega-shear zone separating two contrasting terranes of the Tuareg shield. It is located along the western boundary of the Archaean In Ouzzal rigid terrane, but inside the adjacent Tassendjanet terrane, strongly remobilized at the end of the Precambrian. The Tin Zebane swarm was emplaced during post-collisional sinistral movements along the shear zone at 592.2 ± 5.8 Ma (19WR Rb–Sr isochron). It is a dyke-on-dyke system consisting of dykes and stocks of gabbros and dykes of metaluminous and peralkaline granites. All rock types have Sr and Nd isotopic initial ratios ($Sr_i = 0.7028$ and $\varepsilon_{Nd} = +6.2$) typical of a depleted mantle source, similar to the prevalent mantle (PREMA) at that period. No crustal contamination occurred in the genesis of the Tin Zebane swarm. Even the samples showing evidence of fluid interaction (essentially alkali mobility) have the same isotopic signature. The peralkaline granites have peculiar geochemical characteristics that mimic subduction-related granites: this geochemical signature is interpreted in terms of extensive differentiation effects due to late cumulates comprising aegirine, zircon, titanite, allanite and possibly fergusonite, separated from the liquid in the swarm itself due to magmatic flow turbulence. The Tin Zebane dyke swarm is thus of paramount importance for constraining the differentiation of mantle products to generate highly evolved alkaline granites without continental crust participation, in a post-collisional setting.

Keywords: Alkaline granite; Post-collisional; Pan-African; Prevalent mantle; Tuareg shield; Algeria

1. Introduction

In a post-collisional setting, alkaline magmatism commonly occurs in the form of high-level plutons and dyke swarms that intrude after calc-alkaline magmatism. However, its origin and the reason for its emplacement at that period of an orogenic belt history are still highly debated. The relations be-

* Corresponding author. E-mail: ddemaif@ulb.ac.be
[1] E-mail: zhadj@ulb.ac.be.
[2] E-mail: jplieg@ulb.ac.be.
[3] E-mail: caby@dstu.univ-montp2.fr.

0024-4937/98/$ - see front matter
PII: S0024-4937(98)00033-4

tween the peralkaline and metaluminous alkaline series are also the subject of discussion as are the possible sources of these series, either the continental crust (Clemens et al., 1986) or the mantle (e.g., Bonin, 1996).

Shear zone related dyke complexes from collisional orogens are an important target since they were mostly emplaced during the strike-slip motion (tens or even hundreds of km) of the lateral movement of the terranes. Such large shear zones can be considered as lithospheric faults that may be the locus of drainage of mantle-derived magmas sampled at variable depths. Such shear zones are widespread in the Pan-African rocks of the western part of the Tuareg shield, at about 150 km east of the main suture with the 2 Ga old West African craton. Several alkaline dyke complexes have been described in this domain (Dostal et al., 1979). Among them, the post-collisional group comprises mafic, silica-undersaturated and alkaline–peralkaline rock types.

This study focuses on the Tin Zebane alkaline–peralkaline dyke swarm that intruded after the collision-related HT–HP Pan-African regional metamorphism. It was emplaced during strike-slip movements along N–S trending mega-shear zones that are responsible for the important relative movements of the several terranes constituting the Tuareg shield. The Tin Zebane swarm is thus typically post-collisional.

2. Geological setting

The Tuareg shield is composed of several terranes welded together during the Pan-African orogeny (Black et al., 1994; Fig. 1). It formed during two major collisional periods, an early intense collision with the East Saharan craton at 750–660 Ma, in the East (Black and Liégeois, 1993; Liégeois et al., 1994) and a late more gentle oblique collision with the West African craton at 630–580 Ma, in the West (Black et al., 1979; Caby et al., 1981; Liégeois et al., 1987). These collisions induced large movements along mega-shear zones and mega-basal thrusts inducing in turn important relative displacements between the different terranes (several hundred km; Caby, 1968; Liégeois et al., 1994). The latter are variously composed of Pan-African juvenile rocks with reactivated and/or preserved Archaean–Palaeoproterozoic rocks. Emplacement of widespread calc-alkaline batholiths has accompanied the relative movements (Black et al., 1994). The end of these movements was often marked by the intrusion of high-level plutons, dyke swarms and plateau lavas of alkaline composition (Liégeois and Black, 1987) or of transitional affinity (Azzouni-Sekkal and Boissonnas, 1993). Terrane boundaries are often marked by mafic–ultramafic bodies, potentially ophiolitic, and by late elongated molassic basins (Fig. 1).

The post-collisional alkaline to peralkaline magmatism is mainly located to the west of the shield (Fourcade and Javoy, 1985; Liégeois and Black, 1987). Alkaline magmatism in the central and eastern parts of the shield is either very limited in volume (some facies of the 'Taourirt'-type plutons, Azzouni-Sekkal and Boissonnas, 1993) or much younger than the Pan-African orogeny such as the Aïr ring-complexes at ca. 410 Ma (Moreau et al., 1994) or recent volcanism (Atakor, Girod, 1971; southern Aïr, Moreau et al., 1991). Immediately to the west of the main suture, within the West African craton, the 270–160 Ma Tadhak carbonatite-bearing silica-undersaturated ring-complexes are also younger (Liégeois et al., 1991). Moreover, the post-collisional late Pan-African alkaline magmatism is mainly concentrated within the Kidal and Tassendjanet terranes west of the Archaean granulitic In Ouzzal terrane (Caby, 1996; Fig. 1).

The western branch of the Pan-African Trans-Saharan belt (Kidal terrane in Mali and Tassendjanet terrane in Algeria; Black et al., 1994; Fig. 1) comprises spectacular alkaline dyke swarms in northern Mali (Boullier et al., 1986; Liégeois and Black, 1987). These swarms were emplaced in the rigid, already cooled, Pan-African crust; they are penecontemporaneous to the deposition of molassic series. Their Rb–Sr ages are bracketed between 560 and 540 Ma (Liégeois and Black, 1987; Liégeois et al., 1996). In Western Hoggar, a few alkaline–peralkaline plutons, sometimes associated with calderas, are known (e.g., the In Zize complex; Fourcade and Javoy, 1985 and references therein). On the other hand, older, shear zone related and deformed dyke complexes, considered as late with respect to the regional metamorphism (Caby, 1970) have been de-

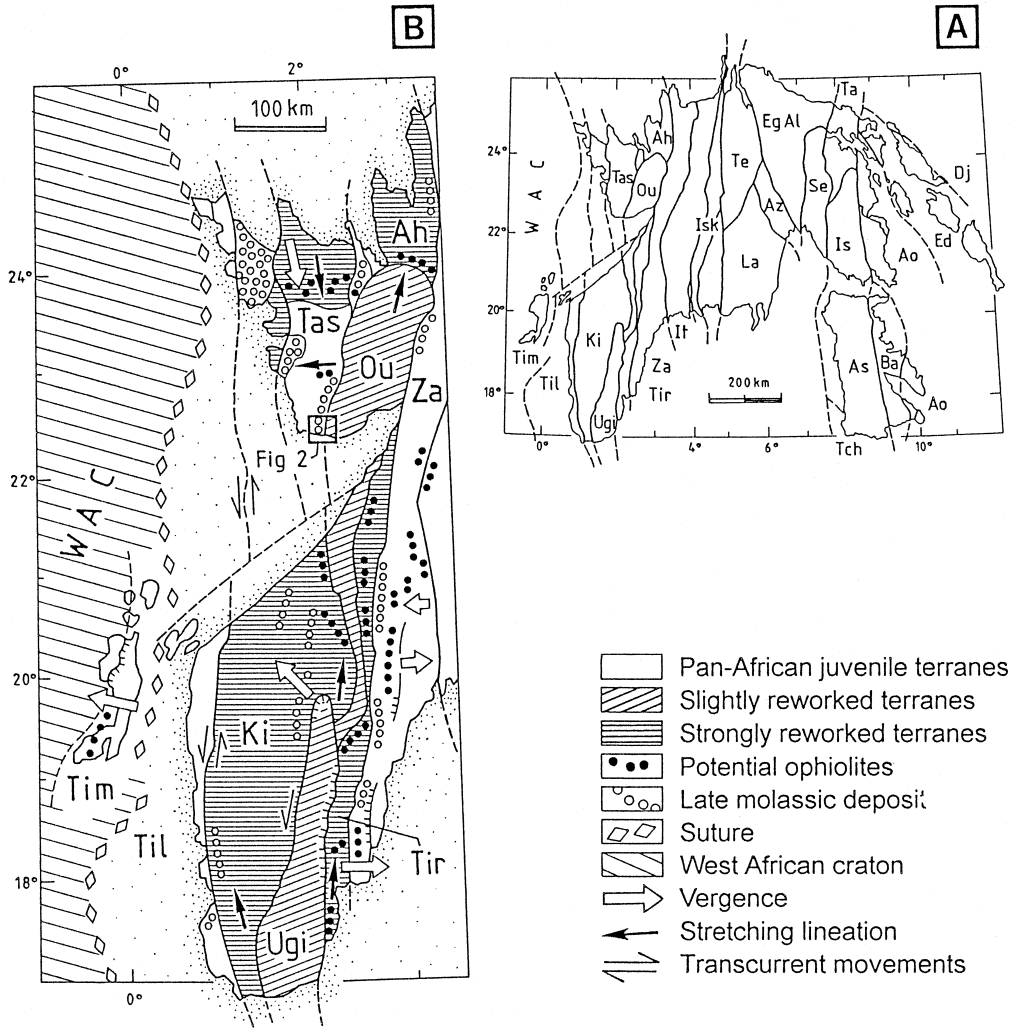

Fig. 1. The Tuareg shield. (A) Sketch map of the Tuareg Shield with terranes boundaries (Black et al., 1994). (B) Western part of the Tuareg shield. Slightly and strongly reworked terranes are made of Archaean and Proterozoic sequences. The suture separates the West African Craton (WAC) from the Tuareg Shield. Ki: Kidal, Ou: In Ouzzal, Tas: Tassendjanet, Til: Tilemsi, Tim: Timetrine, Tir: Tirek, Za: Tin Zaouatene, Ugi: Iforas granulitic unit.

scribed in the same area (Dostal et al., 1979). The Tin Zebane dyke swarm belongs to these complexes.

The Tin Zebane dyke swarm was emplaced at the eastern margin of the Tassendjanet terrane, along a major fault separating it from the In Ouzzal terrane. This sinuous several hundreds km long West Ouzzalian fault is marked in the In Ouzzal only by low-temperature cataclasites and mylonites of several metres to several tens of metres of width at most, while in the Tassendjanet terrane, it is much larger and pervasive (Fig. 2). It had a post-metamorphic sinistral movement of about 150 km (Caby, 1968). The Tassendjanet and In Ouzzal terranes behaved differently during the Pan-African orogeny. The Pan-African imprint was very slight ($T° < 280°C$) in the In Ouzzal terrane which preserved its Palaeoproterozoic ultrahigh temperature (1000°C, Ouzegane and Boumaza, 1996) and granulite facies metamor-

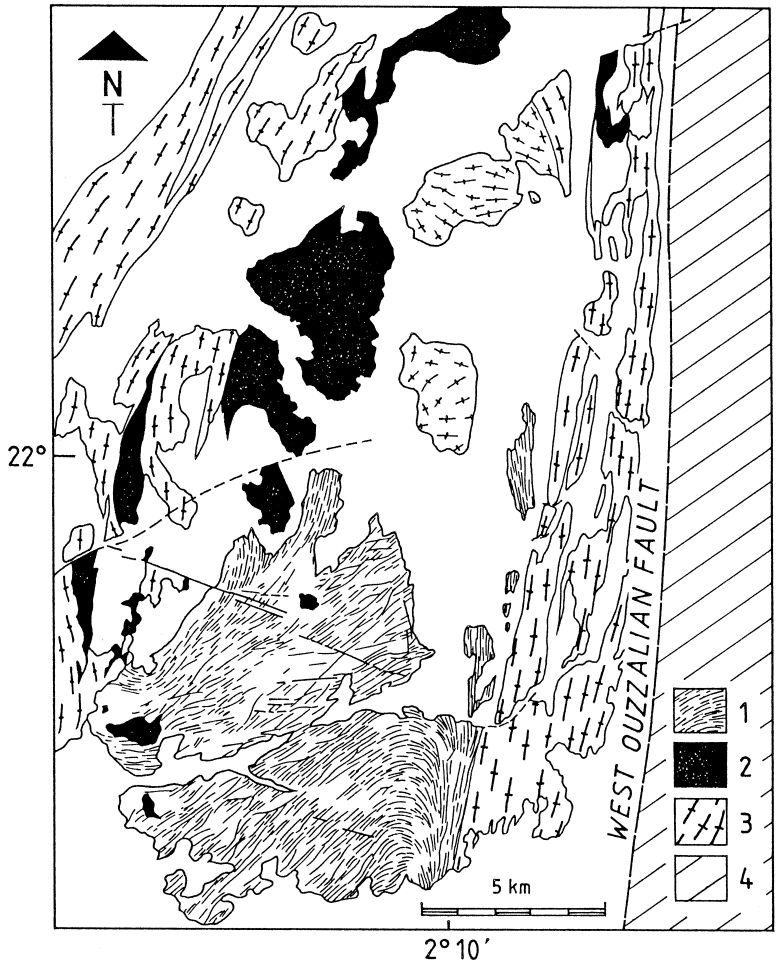

Fig. 2. Geological sketch map of the Tin Zebane area (Dostal et al., 1979). (1) Dyke swarm of Tin Zebane: alkaline–peralkaline granites and pyroxene gabbros and dolerites; (2) main bodies of olivine gabbros; (3) country rocks of the swarm: metasediments and gneisses of Tassendjanet series; (4) Archaean granulitic formation of In Ouzzal.

phic parageneses. This terrane behaved as a rigid cratonic block during the Neoproterozoic; it was most probably attached to its Palaeoproterozoic lithosphere. In contrast, the Pan-African evolution of the Tassendjanet terrane is marked by major thrust sheets, HT–HP metamorphism, abundant magmatism and volcanism (Caby, 1970).

The Tassendjanet terrane, host of the Tin Zebane dyke swarm, recorded nearly the whole Pan-African Wilson cycle. It is composed of (1) an Eburnian gneissic basement in the north, covered by orthoquartzites interleaved with alkaline metarhyolites dated at 1.75 Ga (Caby and Andreopoulos-Renaud, 1983); (2) a ca. 1 Ga Stromatolite series made of quartzites and limestones intruded by (3) thick ultramafic and gabbroic sills (pre-Pan-African oceanic domain at ca. 790 Ma; Dostal et al., 1996) and quartz diorites and granites; (4) thick basaltic to andesitic series (active margin; Chikhaoui et al., 1978; Caby, 1987). These volcanics were reworked to form a thick marine, juvenile Neoproterozoic grauwacke unit with volcanic intercalations (‘Série verte’, 690–630 Ma; Caby et al., 1989). The tectono-metamorphic evolution of monocyclic

metasediments along the In Ouzzal terrane is characterized by an early system of west-verging recumbent folds synchronous with prograde medium temperature mineral assemblages (chloritoid, kyanite, staurolite) in metapelites with the occurrence of retrogressed eclogites in garnet amphibolites, consistent with T° around 550–600°C. (5) Syn-kinematic calc-alkaline plutons correlated with the Iforas batholith (630–580 Ma; Liégeois et al., 1987) intruded to the west with the development of younger high-temperature, low-pressure conditions (Caby, 1987). (6) Exhumation of the root of the Tassendjanet terrane was coeval with infill of continental molassic graben ('Série pourprée') between 570 and 530 Ma.

3. The Tin Zebane dyke swarm

3.1. Field data

The Tin Zebane dyke swarm post-dates the regional HP–HT Pan-African metamorphic event affecting its country-rocks (mainly kyanite-bearing quartzites and schists deposited during the Palaeoproterozoic). It was thus emplaced prior to the brittle tectonics associated with graben development and emplacement of undeformed dyke swarms of alkaline to peralkaline composition (generation V of Dostal et al., 1979). These field relationships indicate an age bracket of 630–540 Ma for the Tin Zebane dykes.

The Tin Zebane dyke complex is a 10 km wide sigmoid dense swarm located along the West Ouzzalian fault at lat. 22°20′N (Fig. 2). It is composed of fine-grained alkaline and peralkaline granites and of gabbros, being then typically bimodal. Intermediate rocks and few rhyolites are recorded but are rare. The dykes are several km in length and from less than one metre to several metres in width. This is a dyke-on-dyke swarm, without any screen of country-rocks. Gabbros from the main body (30 km^2, ca. 5 km thick) display a magmatic layering defined by variable amounts of plagioclase and olivine. The felsic dykes constitute a complex network: they apparently root in stocks and become thinner towards the east, along the fault, where they grade to ultramylonites.

The swarm shows a large open sigmoidal fold. This feature is in agreement with opening tension gashes in a widening transtensional site (Caby, 1970). The large-scale fold/gash is thus considered as syn- to late-magmatic; it is probably connected with the large-scale sinistral displacement along the West Ouzzalian fault. Most felsic rocks were ductilely deformed and partially recrystallized under deep greenschist conditions. This recrystallization occurred during and after the final consolidation of the magma and uplift of the complex.

3.2. Petrography of the dyke swarm

The Tin Zebane dyke swarm is bimodal. Rocks of intermediate composition are very rare. The *basic rocks* are olivine gabbros or pyroxene gabbros and dolerites. Some are completely transformed into greenschist mineral assemblages (calcite–albite–chlorite–actinote–epidote paragenesis). Primary magmatic associations are however preserved in the central part of the main body. *Olivine gabbro* comprises elongated subhedral plagioclase (An_{70-61}), large anhedral olivine (Fo_{66}) rimmed by orthopyroxene (En_{71}), interstitial augite, and abundant Fe–Ti oxides (ilmenite and magnetite) with green spinel. Augite and Fe–Ti oxides are systematically rimmed by hornblende, which also occurs as individual late stage grains. *Pyroxene gabbros and dolerites* are composed of euhedral labradorite laths, subophitic augite, rare orthopyroxene and hornblende, Fe–Ti oxides, titanite and rare apatite. These pyroxene gabbros and dolerites do not present an igneous lamination.

The *coarse-grained felsic rocks* commonly display variously deformed magmatic assemblages. Gradual transition into cataclastic to mylonitic textures can be frequently seen on a few cm scale. The large crystals are deformed and have granulated margins leading to the formation of augen; the fine-grained rocks often show alternating layers or bands of felsic and mafic minerals. Typical porphyroclastic and mylonitic microtextures indicate that solid state deformation occurred after consolidation. However, dykes with undeformed magmatic fabrics have also been observed crosscutting deformed dykes. The syn- to late-kinematic growth of brown or green biotite, riebeckite and aegirine took place during plastic deformation. The secondary mineral associations observed in the retrogressed mafic dykes suggest that the syn-kinematic metamorphism reached deep

greenschist facies conditions following magma solidification.

The acid rocks can be separated into two groups: a peralkaline series characterized by sodic pyroxene and amphibole, and a metaluminous series composed of biotite-bearing fine-grained granite, sometimes with granophyric texture. The *peralkaline granites* are composed of two feldspars (K-feldspar and albite), quartz, sodic clinopyroxene and amphibole with accessory titanite, zircon, apatite, allanite, rutile, ilmenite and magnetite. Rarely preserved perthitic alkali feldspar occurs either as phenocryst or within the mesostasis; it is often partially transformed to microcline with albite rims. The latter is also present as small anhedral to subhedral grains. The quartz, in large or small granulated grains, is always anhedral. The clinopyroxene is an aegirine often with an aegirine–augite core; it forms late interstitial, sometimes poikilitic, elongated crystals or fine needles. It is partly transformed to riebeckite, which occurs also as individual subhedral grains with arfvedsonite cores or as needles. Biotite is rare and present as thin elongated crystals or rimming the sodic amphibole or pyroxene. The *metaluminous granites* have porphyroclastic texture marked by feldspars. The K-feldspar is often a perthitic microcline elongated and granulated. Primary plagioclase is an oligoclase; late albite occurs as rims around microcline. Most samples are subsolvus, sometimes granophyric and some samples contain only albite in the mesostasis. Quartz is late and anhedral. Biotite is ubiquitous but in small amounts; it appears as interstitial elongated crystals associated with the accessory and secondary minerals. Muscovite is well developed in the granophyres as large, presumably primary, elongated crystals while, in other granites, it is scarce and replaces biotite. Only one sample (534.1) contains abundant hornblende. Accessory minerals are titanite, magnetite and ilmenite, primary allanite and clinozoisite, zircon, apatite and rutile. Garnet is rare in biotite granite ($Sp_{42}Gr_{44}Alm_{12}Pyr_1$); it can be abundant in the granophyres where it has a spessartine composition and a clear magmatic habit ($Sp_{50}Gr_{26}Alm_{22}Pyr_2$). Pistachite and fluorine are rare. Secondary chlorite and calcite are common. *Intermediate rocks* are uncommon: one sample of a porphyritic quartz–monzonite is available. It is composed of relict andesine and orthoclase phenocrysts with quartz and accessory minerals (Fe–Ti oxides, zircon and allanite) in a groundmass deeply transformed to greenschist mineral assemblage (clinozoisite, chlorite, quartz, titanite).

One reddish granophyric leucocratic sample (531) contains abundant brick-red microcline both as phenocrysts and in the quartz–feldspar mesostasis. Albite is absent. This rock has suffered subsolidus transformation and fluid interaction, it is classified as 'metasomatic'. Two other samples share unusual abundant microcline relative to the other samples. The first is a devitrified rhyolite (531.2) with slightly perthitic microcline and quartz phenocrysts in a mainly felsic mesostasis. The second (183) is of felsic composition and contains Fe–Mg mineral ghosts (formerly aegirine?); it was probably peralkaline before these subsolidus modifications. Although having different primary features, these three samples have been put together in a '*metasomatic' group* to reflect their common, although at different degrees, subsolidus transformations.

Locally, some dark fine-grained rocks enriched in accessory minerals occur as diffuse layers (few cm thick) in felsic rocks. Sample 538.1 contains abundant quartz, actinolite, rare microcline and over 30% of accessory minerals: mainly zircon (either colourless and inclusion-poor or strongly metamict and Th-rich) but also titanite, allanite, monazite and other REE-rich phosphates and Fe–Ti oxides.

4. Geochronology and isotope geochemistry

4.1. Analytical techniques

After acid digestion of the sample and separation on ion exchange resin, Sr and Nd isotopic measurements have been carried out on a Fisons VG Sector 54 mass spectrometer. All errors are given at the 2σ level. Repeated measurements of Sr and Nd standards have shown that between-run error is better than 0.00002. Systematic measurements of the NBS987 Sr standard during this study gave an average $^{87}Sr/^{86}Sr$ value of 0.710267 ± 0.000007 (normalised to $^{86}Sr/^{88}Sr = 0.1194$). The MERCK Nd standard gave an average $^{143}Nd/^{144}Nd$ value of 0.512742 ± 0.000008 (normalised to $^{146}Nd/^{144}Nd = 0.7219$). Used decay constants (Steiger and Jäger, 1977) are 1.42×10^{-11} yr^{-1} (^{87}Rb) and $6.54\ 10^{-12}$

Table 1
Sr and Nd isotopic ratios

	Sample	Rb	Sr	$^{87}Rb/^{86}Sr$	$^{87}Sr/^{86}Sr$	$2\sigma_m$	Sr_{i592}	Sm	Nd	$^{147}Sm/^{144}Nd$	$^{143}Nd/^{144}Nd$	$2\sigma_m$	ε_{Nd592}	T_{DM}		
														a	b	c
G	188.2	0.50	432	0.0033	0.702834	0.000015	0.702806	0.63	2.20	0.17320	0.512636	0.000045	1.7	1478	2015	1519
G	533	6.35	442	0.0415	0.703151	0.000017	0.702801	1.80	6.80	0.16011	0.512836	0.000009	6.6	675	939	617
QM	532	17.88	183	0.2831	0.705275	0.000011	0.702885	7.00	35.95	0.11777	0.512677	0.000006	6.7	634	776	598
PG	545.1	50.5	10.14	14.596	0.826752	0.000010	0.703539	5.30	23.00	0.13938	0.512709	0.000005	5.7	740	938	701
PG	540.1	56.6	5.90	28.207	0.875178	0.000016	0.637060	5.80	39.00	0.08995	0.512555	0.000005	6.5	641	752	614
PG	546	53.5	7.64	20.599	0.870594	0.000016	0.696698	7.40	51.00	0.08776	0.512542	0.000005	6.4	646	754	619
PG	545.2	63.8	4.52	42.257	1.049651	0.000013	0.692927	10.20	66.00	0.09347	0.512482	0.000004	4.8	745	867	721
PG	269.6	62.0	15.28	11.853	0.799935	0.000013	0.699878	4.60	27.00	0.10305	0.512671	0.000005	7.7	563	680	530
PG	269.4	54.4	20.70	7.648	0.765028	0.000009	0.700465	7.68	53.50	0.08682	0.512586	0.000004	7.3	592	696	563
PG	545	51.4	9.26	16.281	0.835439	0.000018	0.697998	2.10	9.20	0.13806	0.512700	0.000008	5.7	745	939	707
PG	269.2	51.6	4.68	32.621	0.947144	0.000011	0.671760	2.70	14.50	0.11262	0.512589	0.000006	5.4	727	870	697
MG	534.1	92.3	81.2	3.299	0.731801	0.000007	0.703952	5.20	26.00	0.12097	0.512664	0.000007	6.2	673	825	639
MG	526	96.2	38.0	7.358	0.766182	0.000012	0.704063	7.39	35.87	0.12461	0.512700	0.000006	6.7	642	796	605
MG	538.2	72.8	37.6	5.619	0.751109	0.000011	0.703671	7.90	24.00	0.19910	0.512966	0.000005	6.2	959	2167	847
MG	525.1	84.2	13.9	17.725	0.857611	0.000012	0.707982	11.74	56.01	0.12678	0.512758	0.000005	7.6	564	714	522
MGr	531.1	94.0	43.9	6.227	0.757677	0.000009	0.705111	4.80	24.00	0.12097	0.512635	0.000005	5.7	717	873	684
MGr	527.1	74.4	37.4	5.780	0.748905	0.000043	0.700111	9.50	43.00	0.13363	0.512682	0.000005	5.6	356	475	309
MGr	180	67.4	26.2	7.496	0.764841	0.000023	0.701559	8.16	40.87	0.12077	0.512874	0.000006	10.4	739	922	702
mG	183	166	18.73	26.184	0.932882	0.000013	0.711839	9.08	33.65	0.16322	0.512945	0.000010	8.5	429	663	349
mGr	531	235	72.0	9.503	0.780244	0.000011	0.700021	2.49	13.53	0.11131	0.512620	0.000005	6.1	675	812	644
mR	531.2	105	30.2	10.176	0.791142	0.000011	0.705239	5.10	22.00	0.14021	0.512757	0.000006	6.6	659	848	614

Nd and Sr isotopic results. Rb, Sr, Sm and Nd contents in ppm. G = gabbro; QM = quartz monzonite; PG = peralkaline granite; MG = metaluminous granite; MGr = metaluminous granite with granophyric texture; mG = granite from the metasomatic group; mGr = granite with granophyric texture from the metasomatic group; mR = rhyolite from the metasomatic group. Sr_{i592} ($^{87}Sr/^{86}Sr$ initial ratio) and ε_{Nd592} are calculated at 592 Ma, the age of the Rb–Sr isochron. Variability and too low values in Sr_i (< 0.7) are explained by the high Rb/Sr ratio of several samples. The only reliable Sr_i value for Tin Zebane is given by the isochron. Nd model ages (T_{DM}) were calculated following the depleted mantle parameters from Michard et al., 1985 (a), Goldstein et al., 1984 (b) and Nelson and De Paolo, 1985 (c).

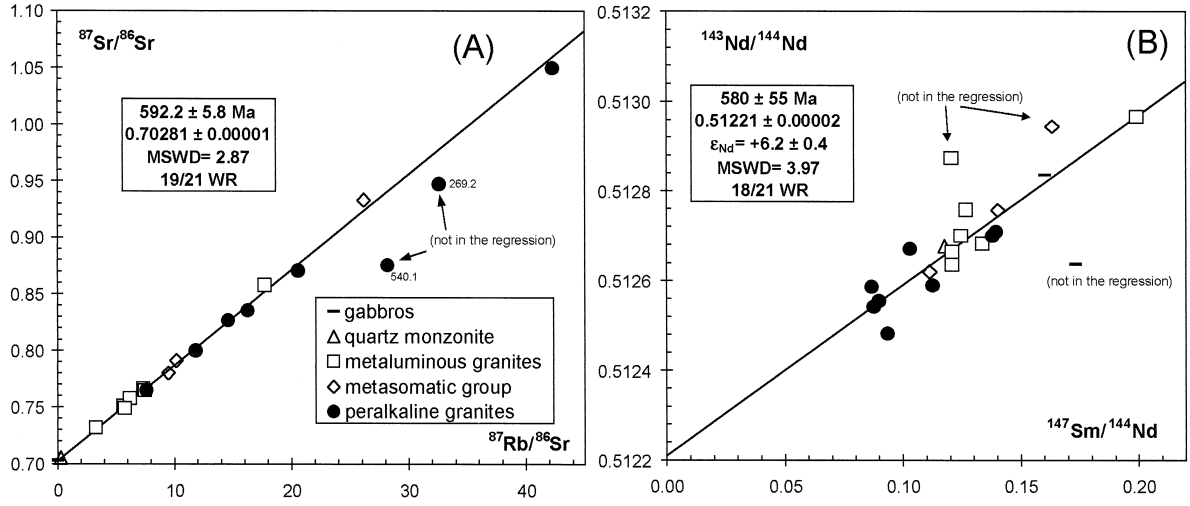

Fig. 3. (A) Rb–Sr isochron diagram. (B) Sm–Nd isochron diagram.

yr^{-1} (^{147}Sm). Isochron calculations were made following Williamson (1968). Results are given in Table 1.

4.2. Results: a PREMA Pan-African mantle production

Twenty-one samples (2 gabbros, 1 quartz monzonite, 7 metaluminous granites, 8 peralkaline granites and 3 'metasomatic' rocks) have been analyzed for the Nd and Sr isotopes (Table 1). Nineteen samples define an isochron in the Rb–Sr isotopic system giving the following parameters: 592.2 ± 5.8 Ma, Sr_i (initial $^{87}Sr/^{86}Sr$) $= 0.70281 \pm 0.00001$ (MSWD = 2.87, 19WR/21; Fig. 3A). In the Sm–Nd isotopic system, despite the narrow range of Sm/Nd ratios, 18 samples form nearly an isochron, giving within error limits an age similar to the Rb–Sr

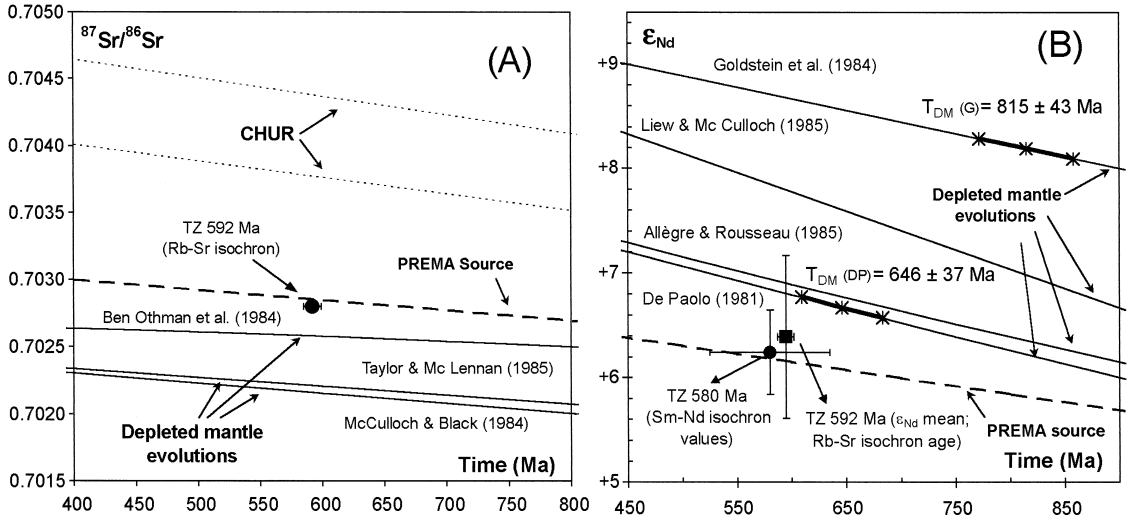

Fig. 4. Position of the Tin Zebane (TZ) isotopic Sr (A) and Nd (B) signatures compared to evolution curves of referenced depleted mantle, prevalent mantle (PREMA) and chondritic uniform reservoir (CHUR). From Allègre and Rousseau (1985), Ben Othman et al. (1984), De Paolo (1981), Goldstein et al. (1984), Liew and McCulloch (1985), McCulloch and Black (1984), Taylor and McLennan (1985) and Zindler and Hart (1986); see a general discussion on these various parameters in Rollinson (1993).

geochronometer: 580 ± 55 Ma, $\varepsilon_{Nd} = +6.2 \pm 0.4$ (MSWD = 3.97, 18WR/21; Fig. 3B).There is no obvious explanation for the outliers in both isotopic systems.

These data show that the different petrographic types of the Tin Zebane dyke swarm, that is the mafic and the felsic rocks, the peralkaline and metaluminous granites, are all cogenetic: they all have the same age and the same source. This source is unusual for granites: the isotopic compositions ($Sr_i = 0.7028$ and $\varepsilon_{Nd} = +6.2$) are indeed characteristic of a rather depleted mantle, even more depleted than the least crust-contaminated sample of the subcontemporaneous Laouni tholeiitic layered intrusion in Central Hoggar ($Sr_i = 0.7029$ and $\varepsilon_{Nd} = +5.1$; Cottin et al., 1998). When compared to different mantle reservoir evolution curves (Fig. 4A and B), the Tin Zebane Nd and Sr initial ratios are only slightly less depleted than the different depleted mantle evolutions. This is reflected by the T_{DM} model ages (Table 1) which are very close to the emplacement age: 646 ± 37 Ma (mean of 18/21 values) with the parameters of Nelson and De Paolo (1985) or slightly older (815 ± 43 Ma, mean of 18/21 values) with the parameters of Goldstein et al. (1984).

The Tin Zebane Nd and Sr initial ratios fall close to the Prevalent Mantle (PREMA) curve. The PREMA component corresponds to a source matching a large proportion of the isotopic characteristics of oceanic basalts (mainly ocean islands), although it does not correspond necessarily to a physical reservoir (Zindler and Hart, 1986). The gabbros, the metaluminous and peralkaline granites of the Tin Zebane dyke swarm come then from a source corresponding to the depleted end-member of the ocean island basalts (OIB) and thus of the alkaline magmatism. This indicates the absence of any contribution of the continental crust. Even a small crustal participation can be ruled out as the Tin Zebane dyke swarm has intruded along the Archaean In Ouzzal terrane which had, at 600 Ma, ε_{Nd} and Sr_i values between -20 and -30 and > 0.720, respectively (calculated from the data of Peucat et al., 1996). This indicates that the northwards motion of the rigid In Ouzzal terrane along the sigmoidal fault created a transtensional site within the rocks of the less rigid Tassendjanet terrane that allows mantle melts to intrude vertically without interaction with the crust.

These isotopic results, in particular the existence of a single Rb–Sr isochron, indicate moreover no or very slight element mobility during penecontemporaneous metamorphism. In the following geochemistry section, metamorphic effect can then be neglected.

5. Major and trace elements geochemistry

5.1. Analytical techniques

Major elements have been measured by X-ray fluorescence spectrometry (XRF) at the University of Liège (CGR-Lambda 2020 instrument) on Li borate discs except Na which was measured on pressed powder pellets (Bologne and Duchesne, 1991). Rb and Sr have been measured by high precision XRF at ULB for concentrations above 10 ppm and by isotope dilution (MRAC-ULB) below 10 ppm. Other trace elements have been measured at MRAC (Section de Géochimie) by ICP-MS (VG PQ2 +): the result of the alkaline fusion (0.3 g of sample + 0.9 g of lithium metaborate at 1000°C during 1 h) has been dissolved in 5% HNO_3. The calibrations were set using both synthetic solution (mixture of the considered elements at 2, 5 and 10 ppb) and international rock standards (BHVO-1, W1, GA, ACE). For all these elements, the precision varies from 5 to 10% (for details, see Navez, 1995). Results are given in Table 2.

5.2. Results

Thirty samples representative of the different petrographical types have been analyzed. Mafic rocks are often retrogressed and/or weathered, only two fresh gabbros have been selected. One intermediate rock only, a quartz monzonite, was available. This study is thus mainly focused on the metaluminous and peralkaline granites. The three samples from the metasomatic group will be also considered.

Both metaluminous and peralkaline series have mean normative compositions close to thermal minimum Ab_{35}–Or_{25}–Q_{40}, suggesting a temperature of 720°C for a pressure of 1 to 2 kbar (Tuttle and Bowen, 1958). All samples have a Na/K molar ratio higher than 1, except the metasomatic group (Fig. 5A). The peralkaline and metaluminous gran-

Table 2
Major and trace element compositions

Sample	Gabbros		Q-mz	Peralkaline granites											
	188.2	533	532	545.1	536	540.1	546	269.5	545.2	269.6	269.4	544	545	540.2	269.2
SiO_2	47.08	47.47	67.09	75.22	76.13	76.16	76.58	76.70	76.78	76.80	76.86	76.88	76.88	77.76	78.08
TiO_2	0.93	1.39	0.46	0.15	0.38	0.20	0.21	0.20	0.20	0.13	0.16	0.22	0.17	0.20	0.17
Al_2O_3	19.41	17.65	15.31	10.92	10.64	11.36	11.21	11.30	11.05	11.30	11.37	11.16	11.07	10.84	11.26
Fe_2O_3	10.72	10.48	4.08	3.22	4.24	2.43	2.31	2.54	2.44	2.53	2.29	2.19	2.62	2.68	1.91
MnO	0.15	0.15	0.06	0.18	0.16	0.10	0.10	0.07	0.09	0.08	0.08	0.10	0.10	0.11	0.07
MgO	7.54	6.92	0.85	0.25	0.09	0.10	0.11	0.08	0.11	0.12	0.05	0.10	0.10	0.08	0.05
CaO	11.63	12.50	1.99	0.26	0.20	0.13	0.21	0.05	0.09	0.20	0.07	0.12	0.11	0.18	0.04
Na_2O	2.26	2.19	7.31	4.54	4.09	4.31	4.00	4.31	4.26	3.59	4.33	3.91	4.19	4.70	3.72
K_2O	1.06	0.23	1.51	4.13	4.00	4.60	4.93	4.52	4.62	5.10	4.43	4.62	4.20	3.06	4.66
P_2O_5	0.03	0.11	0.10	0.05	0.03	0.04	0.02	0.03	0.04	0.04	0.03	0.03	0.03	0.02	0.01
H_2O	0.14	1.09	1.06	0.05	0.34	0.02	0.02	0.05	0.05	0.02	0.40	0.02	0.02	0.02	0.31
Total	99.95	100.2	99.82	98.97	100.3	99.45	99.70	99.85	99.73	99.91	100.1	99.35	99.49	99.65	100.3
A.I.	0.19	0.22	0.89	1.09	1.04	1.06	1.06	1.06	1.09	1.01	1.05	1.02	1.03	1.02	0.99
V	179.0	302.0	41.9	6.1	1.1	1.1	0.7	0.6	0.8	2.1	2.4		3.0	3.3	0.4
Rb	0.5	6.4	17.9	50.6	32.4	56.6	53.5	61.6	63.9	62.0	54.4	46.9	51.5	36.0	51.7
Sr	432.2	442.4	182.7	8.8	10.7	5.9	7.6	23.8	4.5	15.3	20.7	2.1	9.3	7.4	4.7
Y	3.4	8.6	43.7	14.8	5.9	8.1	6.5	7.4	9.8	10.8	12.4		5.4	5.8	4.7
Zr	6.8	27.0	637.7	204.0	24.7	346.0	252.0	376.0	276.0	379.0	324.8		71.0	73.0	282.0
Nb	0.1	0.6	10.1	3.5	1.1	4.8	4.3	6.2	4.7	2.4	5.4		2.0	2.8	3.0
Ba	33	244	634	117	430	217	196	315	148	200	379		131	116	188
La	1.5	4.6	32.7	15.3	33.9	38.0	53.0	42.0	65.0	28.0	58.8		5.5	5.7	14.0
Ce	3.3	9.4	72.3	43.0	69.6	86.0	120.0	89.0	128.0	65.0	124.5		14.5	16.7	30.0
Pr	0.4	1.4	9.0	5.6	7.9	10.5	14.0	12.5	17.0	6.8	14.5		2.0	2.3	3.8
Nd	2.2	6.8	36.0	23.0	29.0	39.0	51.0	46.0	66.0	27.0	53.5		9.2	10.5	14.5
Eu	0.48	0.83	2.03	1.02	0.58	0.93	1.23	1.04	1.65	0.95	1.31		0.45	0.51	0.48
Sm	0.63	1.80	7.00	5.30	3.71	5.80	7.40	6.60	10.20	4.60	7.68		2.10	2.50	2.70
Gd	0.78	2.10	6.42	4.80	2.70	3.60	4.90	3.90	6.90	3.80	5.77		1.90	2.10	2.20
Dy	0.86	2.10	6.54	4.10	1.36	2.40	2.50	2.40	3.30	2.80	2.89		1.58	1.77	1.35
Ho	0.16	0.41	1.31	0.80	0.17	0.42	0.38	0.41	0.54	0.50	0.45		0.26	0.29	0.23
Er	0.46	1.19	3.92	2.40	0.62	1.45	1.07	1.36	1.48	1.45	1.38		0.83	0.92	0.78
Yb	0.43	1.09	4.03	3.90	0.94	2.40	1.34	2.40	2.20	1.56	1.76		1.55	1.48	1.27
Lu	0.06	0.15	0.58	0.75	0.17	0.47	0.25	0.50	0.42	0.24	0.32		0.31	0.28	0.24
Hf	0.29	0.99	14.74	7.90	0.66	6.60	4.90	8.10	5.80	5.90	5.98		2.00	2.60	4.90
Ta	0.10	0.10	0.46	0.24	0.10	0.15	0.10	0.20	0.10	0.10	0.11		0.10	0.10	0.10
W	0.10	0.22	0.10	0.25	0.10	0.59	0.84	0.73	0.50	3.04	0.10		0.96	0.65	0.10
Pb	0.27	5.30	9.19	1.74	2.75	1.88	1.95	0.74	0.69	3.20	2.39		2.20	4.50	1.84
Th	0.12	0.33	5.30	2.00	0.36	2.70	1.59	2.40	1.99	1.97	2.22		0.24	0.41	1.61
U	0.05	0.05	2.00	0.54	0.05	0.49	0.22	0.41	0.36	0.36	0.74		0.09	0.39	0.54

Major and trace element compositions. All major elements in wt.%, all trace elements in ppm. See Table 1 for the affiliation of each sample. Q-mz = quartz monzonite. M.S. = mineral segregation ('magmatic placer' enriched in accessory minerals such as zircon, allanite and titanite). A.I. = Agpaitic index.

ites plot in the same field, the metaluminous granites being slightly more sodic. The peralkaline granites are actually more depleted in Al than enriched in alkalis (Table 2). They have indeed an agpaitic index (AI) above 1 (Fig. 5B) and show a clear negative trend, implying that an alkaline-rich mineral, probably a sodic pyroxene, fractionated from the melt as a late cumulus phase. The most silica enriched peralkaline granite (269.2) has AI slightly lower than 1: this may be marked by the late crystallisation of particu-

Metaluminous granites											Metasomatic granites			M.S.
535	534.1	538	539.1	526	538.2	539.2	525.1	531.1	527.1	180	531	183	531.2	538.1
72.64	74.00	75.80	75.87	76.73	77.16	77.65	78.17	74.65	76.86	77.80	74.77	77.76	77.67	
0.31	0.27	0.15	0.13	0.14	0.11	0.11	0.14	0.23	0.15	0.11	0.17	0.11	0.02	
12.95	13.47	12.48	12.41	11.82	11.51	11.84	10.99	12.58	12.07	12.21	12.61	9.66	12.23	
2.46	1.79	1.41	1.34	1.54	0.75	1.60	2.48	1.66	1.53	1.24	1.42	4.71	0.76	
0.07	0.07	0.04	0.02	0.06	0.07	0.05	0.06	0.03	0.04	0.04	0.02	0.05	0.01	
0.32	0.57	0.24	0.04	0.13	0.12	0.10	0.14	0.23	0.01	0.22	0.04	0.08	0.03	
0.95	0.92	1.07	0.37	0.55	0.55	0.30	0.07	0.50	0.24	0.10	0.36	0.03	0.13	
5.17	5.08	3.70	4.38	4.26	4.40	4.74	4.21	4.35	4.98	4.91	0.17	2.11	2.84	
3.55	4.33	4.53	4.57	4.52	4.34	3.55	3.83	4.47	4.08	3.94	10.83	5.32	6.56	
0.06	0.05	0.04	0.01	0.01	0.03	0.01	0.01	0.04	0.06	0.02	0.06	0.09	0.01	
0.09	0.34	0.05	0.19	0.54	0.08	0.16	0.19	0.10	0.29	0.25	0.05	0.28	0.30	
98.57	100.9	99.51	99.33	100.3	99.12	100.1	100.3	98.84	100.3	100.8	100.5	100.2	100.6	
0.95	0.97	0.88	0.98	1.01	1.04	0.98	1.01	0.95	1.04	1.01	0.95	0.96	0.96	
11.2	9.7		1.1	2.4	3.8	3.1	2.5	4.8	2.6	1.7	22.2	0.4	1.3	26.7
38.8	92.4	102.7	71.0	96.2	72.8	60.0	84.2	94.0	74.4	67.4	234.6	165.8	105.3	3.36
73.9	81.2	101.0		38.1	37.7		14.0	43.9	37.4	26.2	72.0	18.7	30.2	
47.6	28.0		25.0	73.6	74.0	50.0	104.4	26.0	61.0	77.1	22.5	88.5	27.0	4619
315.0	188.0		111.0	301.9	66.0	223.0	763.8	163.0	254.0	339.4	185.4	544.0	72.0	22960
14.8	9.2		10.0	24.2	19.6	9.8	27.7	10.2	19.4	26.1	10.6	18.2	7.9	392
614	383		297	191	487	185	112	379	252	193	774	127	299	197
44.8	27.0		26.0	41.7	17.7	24.0	55.2	26.0	41.0	43.7	19.5	22.2	16.9	2324
100.2	61.0		61.0	97.4	39.0	48.0	125.6	54.0	97.0	94.8	41.4	57.3	45.0	6132
11.9	7.2		6.8	10.1	5.4	5.8	14.7	6.6	11.6	11.3	4.0	7.9	5.7	1047
42.8	26.0		24.0	35.9	24.0	23.0	56.0	24.0	43.0	40.9	13.5	33.7	22.0	4570
1.19	0.80		0.32	0.89	1.23	1.04	1.49	0.57	1.18	0.95	0.31	1.76	0.27	278
8.42	5.20		4.60	7.39	7.90	6.10	11.74	4.80	9.50	8.16	2.49	9.08	5.10	1287
6.39	5.30		4.60	6.98	10.80	7.10	11.43	4.80	9.60	7.67	2.42	9.04	5.00	1198
7.18	6.10		5.40	10.15	15.00	9.50	14.69	5.40	11.70	10.49	3.06	12.33	5.90	1197
1.67	1.28		1.16	2.21	3.20	2.10	3.13	1.17	2.50	2.30	0.69	2.69	1.23	255
4.71	4.00		3.60	7.00	9.00	6.40	9.58	3.60	7.80	7.19	2.17	8.52	3.80	601
5.10	4.40		4.00	7.22	7.20	6.70	9.77	4.00	8.00	7.50	2.56	10.31	4.10	458
0.79	0.64		0.57	1.02	0.87	0.94	1.44	0.56	1.16	1.09	0.37	1.80	0.59	65.8
8.83	7.40		5.60	9.96	2.60	10.10	18.78	6.80	10.20	11.29	5.32	20.17	4.30	549
0.93	1.16		1.10	1.48	2.20	0.98	1.75	1.06	1.66	1.60	0.86	1.17	0.94	47.3
0.61	0.10		0.67	0.10	0.49	0.61	0.14	0.91	0.31	0.18	0.25	2.15	0.10	1.34
13.99	8.80		15.70	8.84	15.20	18.30	13.34	12.20	13.10	12.17	8.73	15.83	15.00	22.9
3.48	9.90		10.40	10.74	4.00	6.20	10.81	10.00	10.20	11.09	11.15	10.64	8.40	324
0.89	3.60		3.70	3.33	0.75	2.31	3.99	3.00	3.56	4.03	3.66	2.83	3.30	87.7

larly abundant biotite rimming aegirine. The metaluminous granites show a positive trend at AI values above 0.87 (the lower limit given by the Iforas alkaline granitoids; Liégeois, 1988), confirming their alkaline metaluminous character. Some metaluminous granites have an AI slightly above 1 although they do not have a peralkaline mineralogy. The two series belong to two converging trends, which induces an overlap of metaluminous and peralkaline granites at high SiO_2 (Fig. 5B). Sample 538 plots distinctly off the metaluminous granite trend: it has a lower agpaitic index (0.88) related to a higher Al/Na

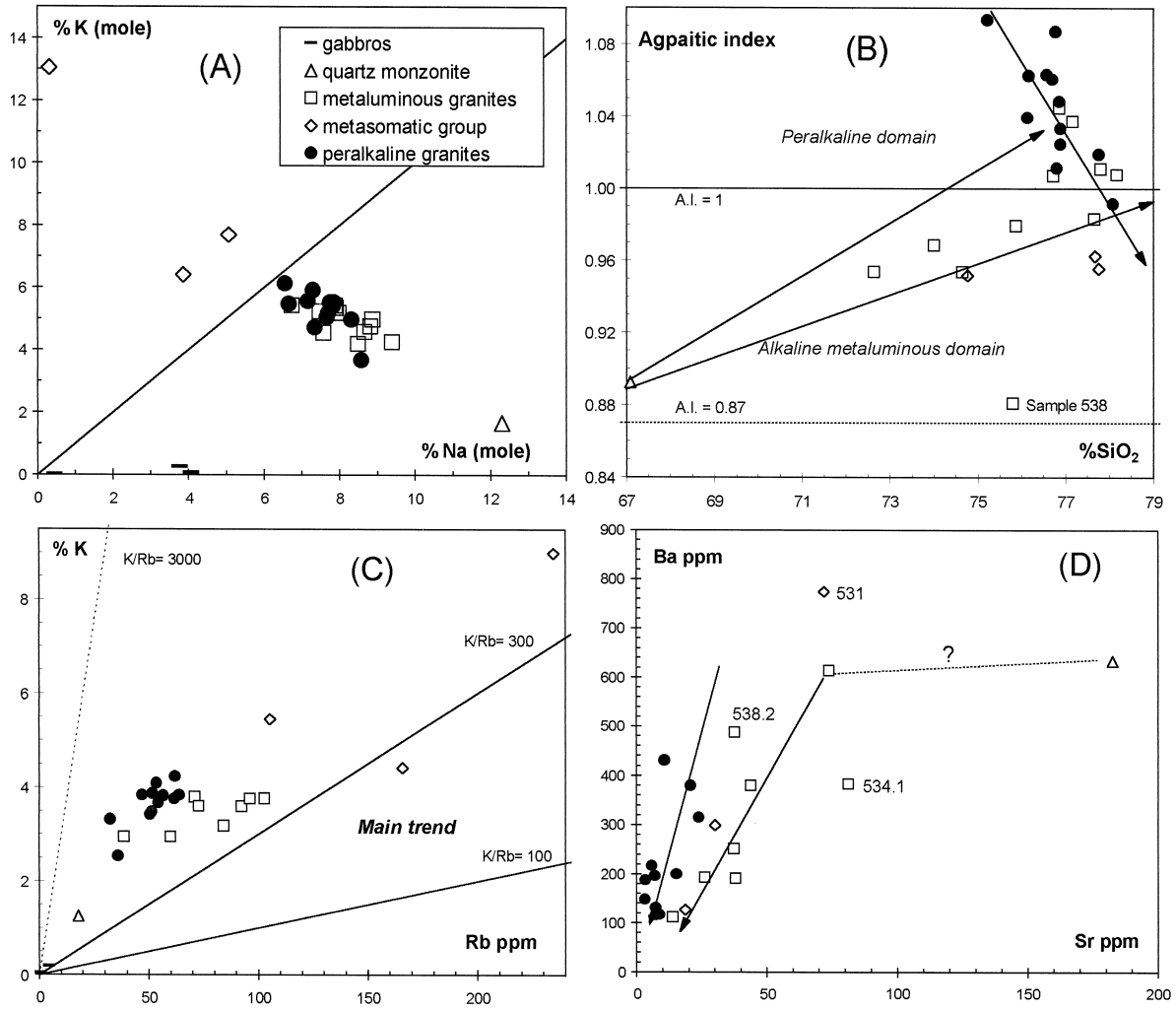

Fig. 5. (A) Molar Na–K diagram showing the similar position of the peralkaline and metaluminous granites (with the latter slightly more sodic, as a mean) and the position in the K domain of the 'metasomatic' group. (B) Silica (wt.%) vs. agpaitic index [(Na + K)/Al, in molar proportions] showing the decreasing trend of the peralkaline series (AI values generally > 1) and the increasing trend of the metaluminous granites (AI values rooted < 1). The lower limit for alkaline granites (0.87) is from Liégeois (1988). (C) Rb ppm vs. % K with the main trend and the K/Rb ratio = 3000 attained in the tholeiitic basalts (Shaw, 1968). (D) Sr vs. Ba (in ppm) showing that the Ba started to decrease at lower values of Sr in the peralkaline series than in the metaluminous one, suggesting a greater plagioclase effect in the former (confirmed by lower Ca and Al).

ratio content. This could be related to the proximity of the accessory mineral-rich pocket (538.1).

In the K–Rb diagram (Fig. 5C), the Tin Zebane samples all plot to the left of the main trend (Shaw, 1968) in the high K/Rb field, at the opposite of the pegmatitic-hydrothermal trend (low K/Rb) that often characterises the strongly differentiated alkaline rocks. The Tin Zebane samples thus have rather low Rb contents suggesting the lack of crustal contamination, Rb being particularly sensitive to this phenomenon (Pearce, 1983). Although having roughly the same potassium content, the peralkaline group appears significantly more depleted in Rb than the metaluminous one. The 'metasomatic' group shows

enrichment in K and in Rb with K/Rb ratios not drastically changed. The peralkaline series (all samples have $> 75\%$ SiO_2) has significantly lower Sr content but similar Ba content than the metaluminous series (Fig. 5D): this could be due to a more important plagioclase effect than in the metaluminous series, in agreement with its rather low Al and Ca contents (Table 2).

The contrasting distributions of major and trace elements between the two groups of felsic rocks (peralkaline and metaluminous) can be further illustrated. The peralkaline series is richer in Fe_2O_3 (Fig. 6A) while Pb and Th are strongly and oddly depleted in the peralkaline granites (Fig. 6B). In Fig. 6A, sample 183 has a Fe_2O_3 content similar to the peralkaline group which can be correlated with its aegirine ghost, while its Pb and Th contents are similar to that of the metaluminous group (Fig. 6B); the two other samples of the metasomatic group belong to the field of the metaluminous group in both diagrams (Fig. 6A,B). This justifies the setup of the two series based on the mineralogy.

In MORB-normalized spidergrams (Fig. 7A–C), the *metaluminous series* (Fig. 7A) shows classical patterns for alkaline rocks: trace element enrichment increases gently with increasing incompatibility of the elements from right to left. Well-defined negative anomalies are observed for Sr, Ba, TiO_2 and P_2O_5; they can be related to the fractionation of plagioclase (Sr), K-feldspar (Ba), apatite (P_2O_5), ilmenite and/or titanite (TiO_2). The quartz monzonite (67% SiO_2) distribution shows that K_2O, Rb, Ta, Nb and HREE behaved as incompatible elements at this stage of the fractionation process, while the others, particularly Sr, P_2O_5, Zr, Hf and TiO_2, behaved compatibly. The subsequent fractionation of plagioclase, apatite, zircon, ilmenite and/or titanite is in agreement with the observed local accumulation of accessory minerals (sample 538.1). The *metasomatic group* (Fig. 7B) has patterns roughly similar to those of the metaluminous granites except for higher K_2O and Rb contents and the relatively low TiO_2. The *peralkaline series* is more peculiar (Fig. 7C): it shows a very deep Sr anomaly (strong plagioclase effect), a small Ba anomaly (moderate K-feldspar fractionation) and important negative anomalies for Nb, Ta, Y and Yb. Samples 536, 540.2 and 545 show that profound depletion in Zr–Hf is linked to that of Th. This could be related to the Th-rich zircon of the accessory minerals-rich rock (538.1; Table 2).

Chondrite-normalized REE spectra of the peralkaline rocks are also very peculiar (Fig. 8A): they are variably enriched in LREE (La_N from 15 to 180) and strongly depleted in heavy REE (HREE), more in the intermediate ones (Ho_N and $Er_N < 10$) than in Yb and Lu, so that the pattern has a positive slope in the HREE. They also have a negative Eu anomalies ($Eu/Eu* = 0.56–0.69$). The three Zr–Hf–Th depleted samples (536, 540.2, 545) are among the most HREE depleted samples, enhancing the zircon effect.

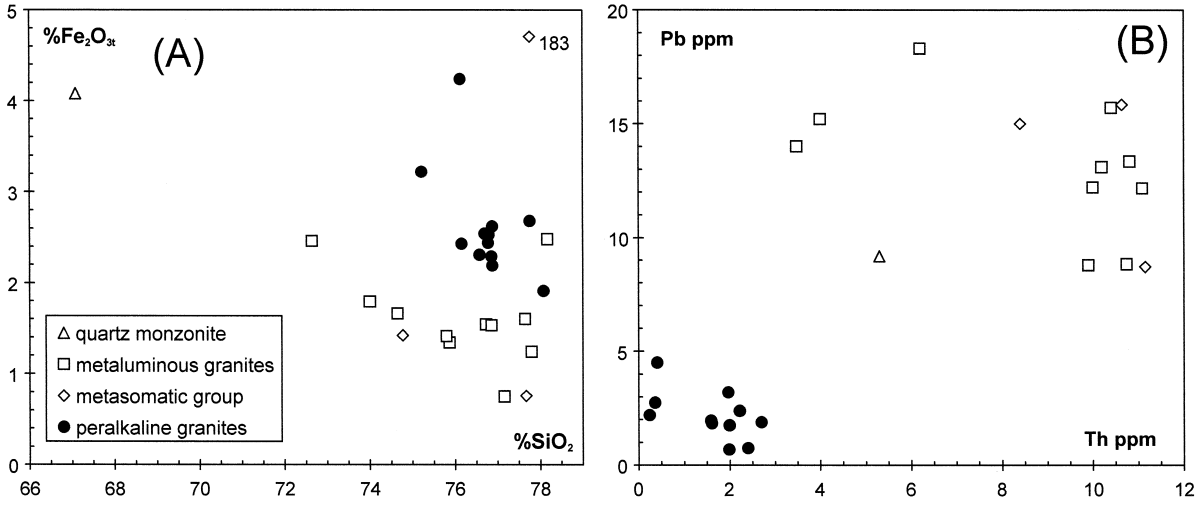

Fig. 6. SiO_2 vs. Fe_2O_{3t} (A) and Th vs. Pb (B) showing important chemical differences between the peralkaline and metaluminous series.

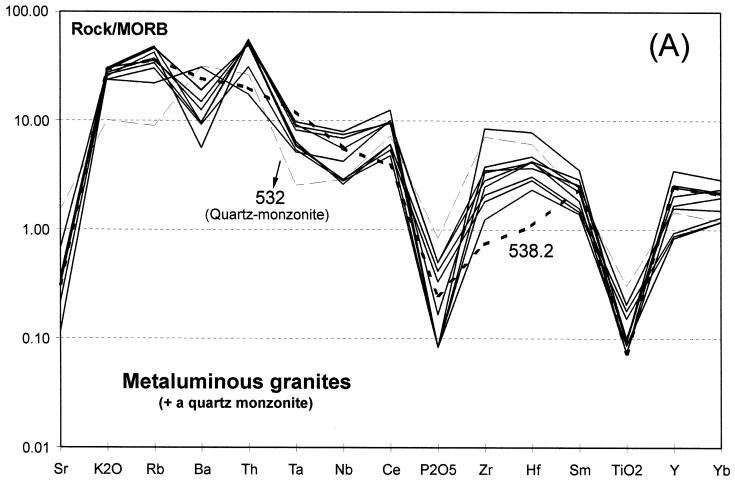
100.00
10.00
1.00
0.10
0.01
Rock/MORB
(A)
532
(Quartz-monzonite)
538.2
Metaluminous granites
(+ a quartz monzonite)
Sr K2O Rb Ba Th Ta Nb Ce P2O5 Zr Hf Sm TiO2 Y Yb

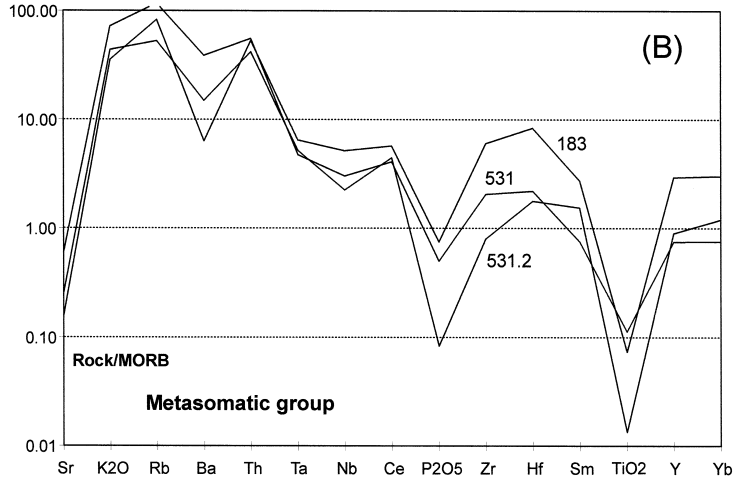
100.00
10.00
1.00
0.10
0.01
(B)
183
531
531.2
Rock/MORB
Metasomatic group
Sr K2O Rb Ba Th Ta Nb Ce P2O5 Zr Hf Sm TiO2 Y Yb

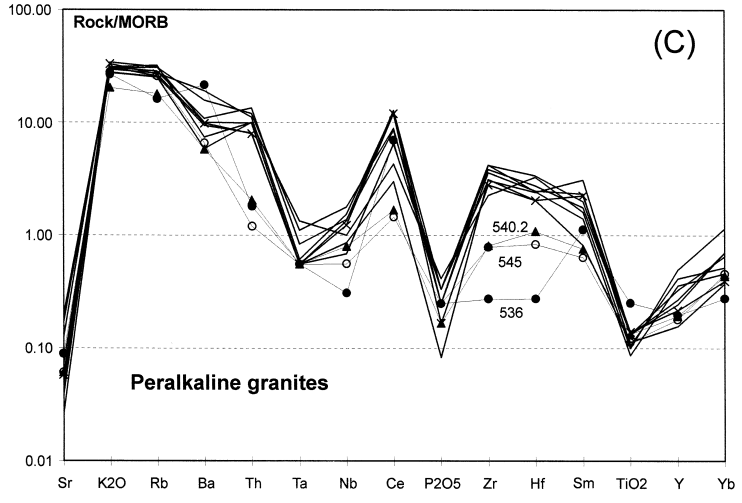
100.00
10.00
1.00
0.10
0.01
Rock/MORB
(C)
540.2
545
536
Peralkaline granites
Sr K2O Rb Ba Th Ta Nb Ce P2O5 Zr Hf Sm TiO2 Y Yb

The negative anomaly in Ho–Er is not correlated to the HREE abundance and then not to zircon fractionation. The LREE depletion of samples 540.2 and 545 can be related to allanite fractionation, which is associated with zircon in sample 538.1, while sample 536 was not so affected. The metaluminous series displays more typical alkaline patterns (Fig. 8B) with flat and enriched HREE (15 to 40 × chondrites), concave LREE and important negative Eu anomalies ($Eu/Eu* = 0.16–0.51$). It is noteworthy that the absolute Eu contents are similar in both series (Fig. 9B): the $Eu/Eu*$ ratio is higher in the peralkaline series due the general lowering of the other REEs during late agpaitic differentiation. This late magma evolution, in which feldspars do not play any role, only slightly affects Eu and balances the early strong plagioclase effect supposed to be responsible for the peralkalinity of the series. The metasomatic group displays spectra roughly similar to the metaluminous ones: the range of values is nevertheless quite large with the 'seagull' pattern of sample 183 and the low abundances of HREE in sample 531. Interestingly, they do not have the peculiar patterns of the peralkaline group, indicating that the Na–K subsolidus metasomatism is not at the origin of the REE spectra of the peralkaline rocks, which is then not comparable to what has been described for the Younger Granites in Nigeria (Kinnaird and Bowden, 1985).

5.3. A late agpaitic differentiation due to magmatic flow turbulence

What can then be the causes of the peculiar trace element distributions of the peralkaline series? Several arguments suggest that advanced magmatic differentiation has played an important role: (1) the rocks are all highly differentiated, with SiO_2 contents in the range 75–78% (Table 2); (2) the decrease of the agpaitic index (Fig. 5B) suggests that a late alkali-rich mineral such as a sodic pyroxene crystallized and separated from the liquid; (3) the REE content as a whole is variable and can be low ($\sum REE = 40–303$ ppm; by comparison metaluminous granites have $\sum REE = 92–314$ ppm), while HREE are always low ($\sum Dy–Lu = 3.9–11.9$ ppm) compared to metaluminous granites (14.7–35.6 ppm). This suggests that accessory REE-rich phases (particularly HREE-rich) could have accompanied the Na–pyroxene fractionation; (4) The accessory minerals-rich rock (sample 538.1) occurring in the Tin Zebane dyke swarm has very high concentrations of incompatible elements (22960 ppm Zr, 1197 ppm Dy, 47 ppm Ta, etc.; Table 2). This indicates that the emplacement of the magma in the dyke system allows the late separation of such phases, which can in turn drive the liquid composition; (5) Except the late greenschist mineral assemblage, no traces of post-magmatic phases are seen.

However, the depletion observed for several trace elements (i.e., Zr, Hf, Th, Ho, Er) in the Tin Zebane peralkaline series requires further examination: indeed, fractionation of the accessory minerals found in sample 538.1 cannot explain the whole peralkaline spidergram pattern: sample 538.2 that is in close contact with segregation 538.1. is characterized by a depletion in Zr–Hf (Fig. 7A) due to the high proportion of zircon in the nearby segregation but lacks negative Ba, Nb, Ta, Ho, Er anomalies characteristic of the peralkaline series. Indeed, 538.1 segregation does not possess the required Nb–Ta and Ho–Er positive anomalies. However, the occurrence of this accessory minerals-rich late cumulate is a major argument in favour of cumulative phenomena during emplacement, either through a filter-press at depth or through dynamic concentrations in the swarm itself due to magmatic flow turbulence within the dyke conduit. In that respect, sample 538.1 could be described as a 'magmatic placer'. The strong Nb–Ta negative anomaly of the peralkaline series suggests the fractionation of additional accessory phases rich in these elements like minerals of the fergusonite–formanite series ($REEYThU(Nb,Ta)O_4$): this mineral will obviously deplete the residual liquid in Nb–Ta but also in intermediate HREE as it is strongly enriched in these elements (Fig. 9B; Bea, 1996). Nb–Ta ore minerals associated with late granites are

Fig. 7. Spidergrams normalised to MORB (Pearce et al., 1981) for the metaluminous granites (A), the 'metasomatic' group (B) and the peralkaline granites (C). Note the Nb–Ta negative anomaly, the positive slope of Y–Yb and the low abundance of Sr in the peralkaline granites. The 'metasomatic' group is not very different from the metaluminous granites.

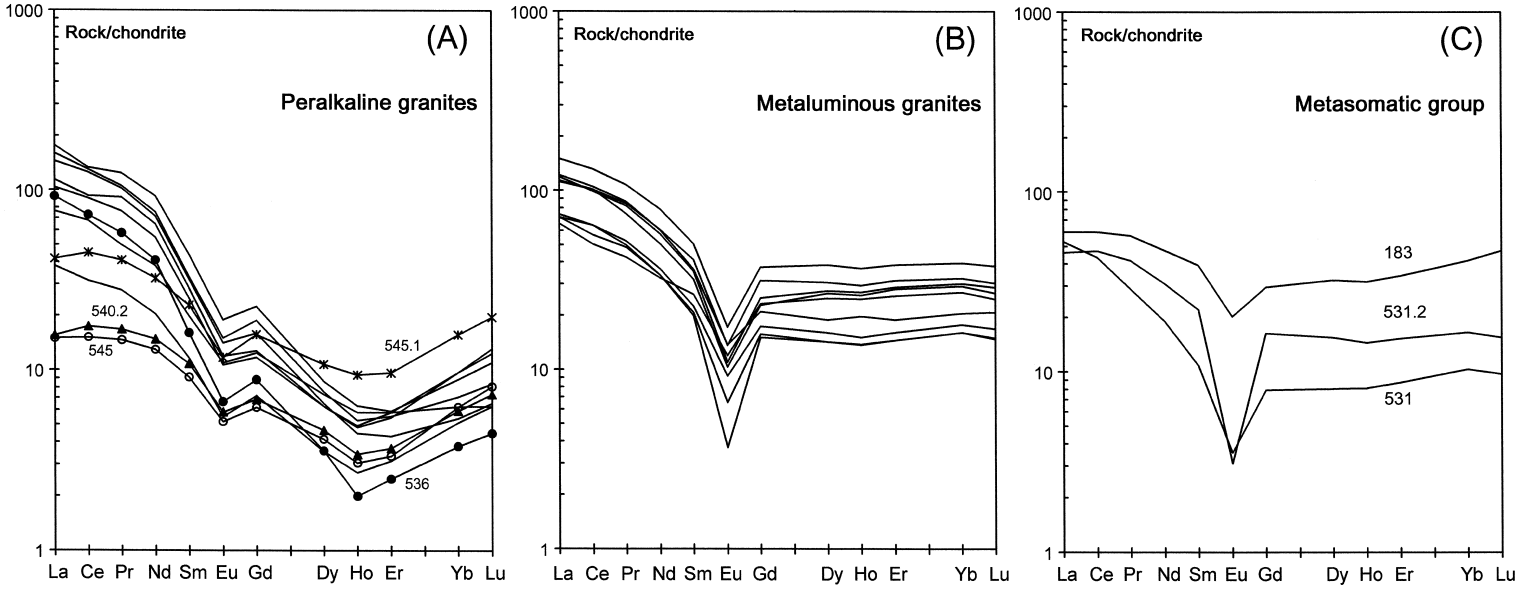

Fig. 8. Chondrite-normalized Rare Earth Elements abundances (Taylor and McLennan, 1985) for peralkaline granites (A), metaluminous granites (B) and the 'metasomatic' group (C). Remark the peculiar spectra of the peralkaline group (lowering of all REE, particularly Ho and Er inducing a positive slope for the HREE) interpreted as the result of a late agpaitic differentiation (see text).

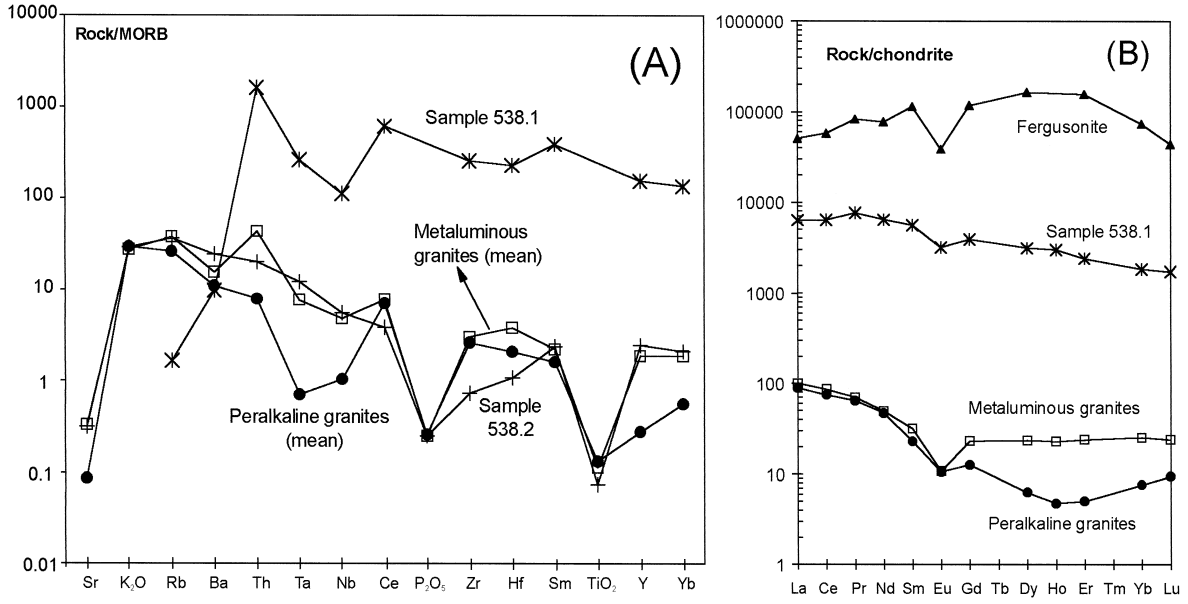

Fig. 9. Spidergrams normalised to MORB (A) and chondrite-normalized REE abundances (B) for the mean of the peralkaline and metaluminous granites, the accessory minerals enriched segregation (sample 538.1) and for the fergusonite (Bea, 1996). Such segregation and in particular the fergusonite have probably played an important role in the late differentiation of the peralkaline series.

well known in Hoggar and fergusonite has been reported in the alkaline facies of the late Pan-African 'Taourirt' plutons in Hoggar (Azzouni-Sekkal and Bonin, 1998) and in alkaline complexes in Aïr (Moreau et al., 1991).

So, after an early phase of plagioclase accumulation (the 'plagioclase effect') which could generate anorthosite (as in Aïr ring-complexes of N. Niger; Black, 1965; Demaiffe et al., 1991a,b) and lead to an Al depletion, later cumulates containing plagioclase, K-feldspar, aegirine, trace element-rich accessory minerals in variable proportions could lead from a 'normal' alkaline composition to the pattern of the Tin Zebane peralkaline series (Fig. 9A,B). In particular, fractionation of fergusonite–formanite and of Zr-rich minerals (zircon, Zr-silicates) seems necessary to explain the Zr–Hf, Nb–Ta and intermediate HREE depletion of the peralkaline granites. The proportion of these minerals in the late cumulate can vary quite largely as shown by samples 536, 540.2 and 545 (Fig. 7C; Fig. 8A), which can be explained by a mechanical flow turbulence-induced separation. This phenomenon can be particularly efficient in peralkaline silicic magmas which can be extremely fluid if containing a few percent of F and H_2O (Dingwell et al., 1998). These volatiles moreover favours more efficient crystallization–fractionation in peralkaline granitic melts (Baker and Vaillancourt, 1995).

The late-stage fractionation of peculiar accessory minerals is thus responsible of depletion of the peralkaline granites in trace elements like Nb–Ta and HREE. This depletion is also characteristic of subduction related-magmas. That is why the Tin Zebane peralkaline series lies in the 'wrong field' in geochemical diagrams discriminating tectonic setting using these elements (Fig. 10A). In other diagrams, only the major elements are discriminant for the peralkaline series (Fig. 10B) while the metaluminous series is often in an ambiguous position (Fig. 10A,B). In the La_N/Yb_N vs. Yb diagram (Fig. 10C; Martin, 1987), the juvenile Tin Zebane Pan-African peralkaline series follows an Archaean trend, again a result of the late agpaitic differentiation, while the metaluminous and metasomatic groups are more conventional (modern style). These types of diagrams can

bring useful information, but only if the domains are regarded as representing classical rock-types and not as absolute tectonic setting references.

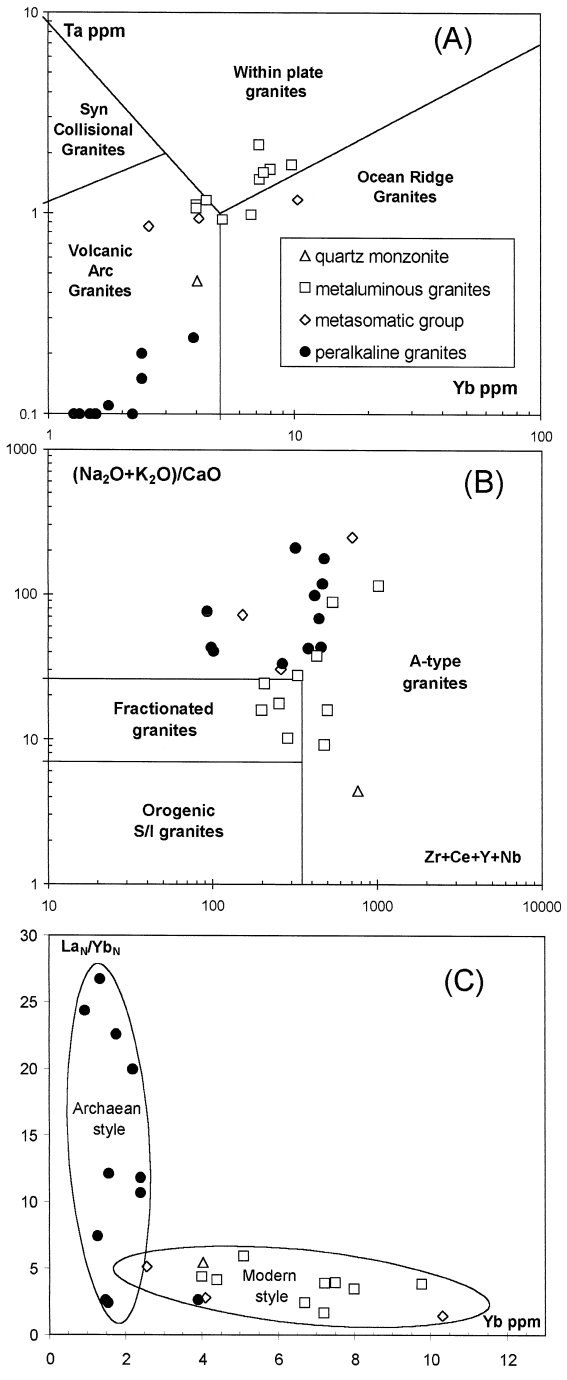

Fig. 10. Discrimination diagrams showing that the late agpaitic differentiation has given to the Pan-African post-collisional juvenile peralkaline Tin Zebane series some 'subduction-like' chemical signature (A; Pearce et al., 1984), the A-type being given by the major elements (B; Whalen et al., 1987), or an Archaean style (C; Martin, 1987). The metaluminous series gives ambiguous answers in the first two diagrams (A,B).

6. General discussion and conclusions

The Tin Zebane dyke swarm was emplaced at 592.2 ± 5.8 Ma (Rb–Sr 19WR isochron) along a shear zone separating a cratonic Archaean terrane and a highly rejuvenated terrane. Depleted mantle model ages (T_{DM}) are only slightly older than the emplacement age, varying from 646 ± 37 to 815 ± 43 Ma following the parameters used; these data are in agreement with Sr and Nd initial ratios ($Sr_i = 0.70281 \pm 0.00001$; $\varepsilon_{Nd} = +6.4 \pm 0.6$ at 592 Ma) that plot in the depleted mantle quadrant for all types of rocks, mafic and felsic, peralkaline and metaluminous. Both Nd and Sr initial ratios are in the range of the prevalent mantle source (PREMA; Zindler and Hart, 1986), calculated back to 592 Ma, pointing to a depleted OIB-type mantle source. Although PREMA is probably not a physically distinct reservoir, the observed isotopic characteristics favour the important role of an asthenospheric source (Zindler and Hart, 1986; Black and Liégeois, 1993). This isotopic signature can be related to a rapid upwelling of the asthenosphere under the lithospheric fault following a linear and local delamination of the lithosphere. This rapid upwelling could induce a partial melting of the asthenosphere by pressure release accompanied possibly by a partial melting of the hotter lithosphere, i.e., the lowest and youngest lithosphere, which can be enriched in OIB-type components (Black and Liégeois, 1993).

Crustal contamination, even a slight one, is considered to be unlikely, as the country-rocks are either the Archaean In Ouzzal terrane with highly radiogenic signatures at 600 Ma (Peucat et al., 1996) or Palaeoproterozoic terrigeneous metasediments. Moreover, the 'metasomatic' group of rocks identified in the Tin Zebane swarm, which shows evidence of interaction with fluids (enrichment in K, loss of Na) has kept the same Nd and Sr initial ratios. This

indicates that the dyke swarm behaved as a closed system even for late-magmatic fluids.

The availability of the PREMA source to generate the Tin Zebane parental magma could be linked to a rapid thinning of the lithospheric mantle under the shear zone by delamination (Black and Liégeois, 1993), allowing the asthenosphere to rise and to melt. This phenomenon had to be of rather small volume and short time to preclude any melting of the continental crust: moreover, tectonic movements had to allow a rapid ascent of the magma. These two factors could be related to the cratonic character (= thick lithospheric mantle; Black and Liégeois, 1993) of the In Ouzzal terrane, whose stiffness can create room for uprising mantle magma along its contact with the less rigid Tassendjanet terrane, but whose cold crust will hardly melt. Post-collisional movements along shear zones were then essential for the generation and ascent of the Tin Zebane dyke swarm.

The bimodal character of the Tin Zebane dyke swarm (gabbroic cumulates and granitic melts) could be matched by an intermediate composition of the parental mantle, as suggested by Lameyre and Bonin (1978). The problem of the localisation of important amounts of mafic–ultramafic rocks necessary to produce the Tin Zebane granites can be easily met if a detachment of the lithospheric mantle occurred under the shear zone.

As the two felsic series, peralkaline and metaluminous, have the same Sr and Nd isotopic compositions, which are moreover similar to those of the mafic rocks, the whole dyke swarm appears to be derived from the same mantle source. The question of how and when the divergence between the two felsic series started cannot definitely be answered with available data. Trace element composition precludes however the derivation of one granitic series from the other, so that the divergence had started before the granitic stage and even earlier, if the quartz monzonite, which seems to belong to the metaluminous series, is taken into account. More data on mafic rocks would be necessary to constraint more precisely their origin and link with the granites.

The peralkaline series shows evidence for a larger plagioclase effect than the metaluminous series: this is marked by lower Ca, Sr and Al contents. The late differentiation of the peralkaline series provoked the development of peculiar features in the trace element distribution such as a negative Nb–Ta anomaly and low HREE (particularly Er and Ho) abundance. Local accumulation of accessory phases such as zircon, allanite, titanite and probably fergusonite accompanied by aegirine can account for this signature. Major elements have been only slightly affected by this late fractionation process, the most prominent feature being the decrease of the agpaitic index with increasing SiO_2. This late cumulate probably segregated from the melt due to fluid turbulence within the dyke system and could be described as a 'magmatic placer'. It is notable that some of the geochemical features of the peralkaline series acquired during this late agpaitic differentiation mimic a subduction-related signature.

Acknowledgements

ZHK thanks the Belgian 'Administration Générale pour la Coopération au Développement' (AGCD) for the grant allowing her to realise a thesis on the Hoggar geology. J. Dostal and C. Moreau are thanked for their constructive reviews.

References

Allègre, C.J., Rousseau, D., 1985. The growth of the continents through geological time studied by the Nd isotopic analysis of shales. Earth Planet. Sci. Lett. 67, 19–34.

Azzouni-Sekkal, A., Boissonnas, J., 1993. Une province magmatique de transition du calco-alcalin à l'alcalin: les granitoïdes pan-africains à structures annulaires de la chaîne pharusienne du Hoggar (Algérie). Bull. Soc. Géol. Fr. 164, 597–608.

Azzouni-Sekkal, A., Bonin, B., 1998. Les minéraux accessoires des granitoïdes de la suite 'taourirt', Hoggar, (Algérie): conséquences pétrogénétiques. J. Afr. Earth Sci. 26, 65–87.

Baker, D.R., Vaillancourt, J., 1995. The low viscosities of F+H_2O-bearing granitic melts and implications for melt extraction and transport. Earth Planet. Sci. Lett. 132, 199–211.

Bea, F., 1996. Residence of REE, Y, Th and U in granites and crustal protoliths: implications for the chemistry of crustal melts. J. Petrol. 37, 521–552.

Ben Othman, D., Polvé, M., Allègre, C.J., 1984. Nd–Sr isotopic composition of granulites and constraints on the evolution of the lower continental crust. Nature 307, 510–515.

Black, R., 1965. Sur la signification pétrogénétique de la découverte d'anorthosites associées aux complexes annulaires sub-volcaniques du Niger. C.R. Acad. Sci. Paris 260, 5829–5832.

Black, R., Liégeois, J.P., 1993. Cratons, mobile belts, alkaline rocks and continental lithospheric mantle: the Pan-African testimony. J. Geol. Soc. London 150, 89–98.

Black, R., Caby, R., Moussine-Pouchkine, A., Bayer, R., Bertrand, J.M.L., Boullier, A.M., Fabre, J., Lesquer, A., 1979. Evidence for late Precambrian plate tectonics in West Africa. Nature 278, 223–227.

Black, R., Latouche, L., Liégeois, J.P., Caby, R., Bertrand, J.M., 1994. Pan-African displaced terranes in the Tuareg shield (central Sahara). Geology 22, 641–644.

Bologne, G., Duchesne, J.C., 1991. Analyse des roches silicatées par spectrométrie de fluorescence X: précision et exactitude. Belgian Geol. Survey Prof. Pap. 249, 1–11.

Bonin, B. 1996. A-type granite ring-complexes: mantle origin through crustal filters and the anorthosite–rapakivi magmatism connection. In: Demaiffe, D. (Ed.), Petrology and Geochemistry of Magmatic Suite of Rocks in the Continental and Oceanic crusts. ULB-MRAC, Bruxelles, pp. 201–218.

Boullier, A.M., Liégeois, J.P., Black, R., Fabre, J., Sauvage, M., Bertrand, J.M., 1986. Late Pan-African tectonics marking the transition from subduction-related calc-alkaline magmatism to within-plate alkaline granitoids (Adrar des Iforas, Mali). Tectonophysics 132, 233–246.

Caby, R., 1968. Une zone de décrochement à l'échelle de l'Afrique dans le Précambrien de l'Ahaggar occidental. Bull. Soc. Geol. Fr. 10, 577–587.

Caby, R., 1970. La chaine pharusienne dans le NW de l'Ahaggar (Sahara central; Algérie): sa place dans l'orogenèse du Précambrien supérieur en Afrique. Thesis, University of Montpellier and 1983, Publication de la Direction des Mines et de la Géologie, Algiers, 47, 289 pp.

Caby, R., 1987. The pan-African belt of west Africa from the Sahara Desert to the Gulf of Benin. In: Schaer, J.P., Rodgers, J. (Eds.), Anatomy of mountain ranges. Princeton University Press, Princeton, NJ, pp. 129–170.

Caby, R., 1996. A review of the In Ouzzal granulitic terrane (Tuareg shield, Algeria): its significance within the Pan-African Trans-Saharan belt. J. Metam. Geol. 14, 659–666.

Caby, R., Andreopoulos-Renaud, U., 1983. Age à 1800 Ma du magmatisme sub-alcalin associé aux métasédiments monocycliques dans la chaîne pan-africaine du Sahara central. J. Afr. Earth Sci. 1, 193–197.

Caby, R., Bertrand, J.M., Black, R., 1981. Pan-African closure and continental collision in the Hoggar–Iforas segment, Central Sahara. In: Kröner, A. (Ed.), Precambrian Plate Tectonics. Elsevier, Amsterdam, pp. 407–434.

Caby, R., Andreopoulos-Renaud, U., Pin, C., 1989. Late Proterozoic arc-continent and continent–continent collision in the Pan-African Trans-Saharan belt of Mali. Can. J. Earth Sci. 26, 1136–1146.

Chikhaoui, M., Dupuy, C., Dostal, J., 1978. Geochemistry of late Proterozoic volcanic rocks from Tassendjanet area (NW Hoggar, Algeria). Contrib. Mineral. Petrol. 66, 157–164.

Clemens, J.D., Holloway, J.R., White, A.J.R., 1986. Origin of an A-type granite: experimental constraints. Am. Mineral. 71, 317–324.

Cottin, J.Y., Lorand, J.P., Agrinier, P., Liégeois, J.P., Bodinier, J.L., 1998. Isotopic (O, Sr, Nd) and trace element geochemistry of the Laouni layered intrusions (Pan-African belt, Hoggar, Algeria): evidence for post-collisional continental tholeiitic magmas variably contaminated by continental crust. Lithos, this volume.

Demaiffe, D., Moreau, C., Brown, W.L., 1991a. Ring-complexes of Ofoud-type in Aïr, Niger: a new anorogenic-type anorthosite association. In: Kampunzu, A.B., Lubala, R.T. (Eds.), Magmatism in extensional structural settings. The Phanerozoic African plate. Springer Verlag, Berlin, pp. 353–376.

Demaiffe, D., Moreau, C., Brown, B., Weis, D., 1991b. Geochemical and isotopic (Sr, Nd and Pb) evidence on the origin of the anorthosite-bearing anorogenic complexes of the Aïr Province, Niger. Earth Planet. Sci. Lett. 105, 28–46.

De Paolo, D.J., 1981. Neodymium isotopes in the Colorado Front range and crust–mantle evolution in the Proterozoic. Nature 291, 193–196.

Dingwell, D.B., Hess, K.U., Romano, C., 1998. Extremely fluid behavior of hydrous peralkaline rhyolites. Earth Planet. Sci. Lett. 158, 31–38.

Dostal, J., Caby, R., Dupuy, C., 1979. Metamorphosed alkaline intrusions and dyke complexes within the Pan-African belt of western Hoggar (Algeria): geology and geochemistry. Precambr. Res. 10, 1–20.

Dostal, J., Caby, R., Dupuy, C., Mével, C., Owen, J.V., 1996. Inception and demise of a Pre-Pan-African ocean basin: evidence from the Ougda complex, western Hoggar (Algeria). Geol. Rundsch. 85, 619–631.

Fourcade, S., Javoy, M., 1985. Preliminary investigations of $^{18}O/^{16}O$ and D/H compositions in rhyo-ignimbrites in the In Hihaou (In Zize) magmatic center, central Algeria. Contrib. Mineral. Petrol. 89, 285–295.

Girod, M., 1971. Le massif volcanique de l'Atakor (Hoggar, Sahara algérien). Mémoire CRZA, Série Géol., éd. CNRS, Paris, 12, 155 pp.

Goldstein, S.L., O'Nions, R.K., Hamilton, P.J., 1984. A Sr–Nd study of atmospheric dusts and particulates from major river systems. Earth Planet. Sci. Lett. 70, 221–236.

Kinnaird, J., Bowden, P., 1985. African anorogenic alkaline magmatism and mineralization—a discussion with reference to the Niger–Nigerian province. Geol. J. 22, 297–340.

Lameyre, J., Bonin, B., 1978. Réflexions sur la position et l'origine des complexes magmatiques anorogéniques. Bull. Soc. Geol. Fr. 20, 45–59.

Liégeois, J.P., 1988. Le batholite composite de l'Adrar des Iforas (Mali). Académie royale des Sciences d'Outre-Mer, Classe des Sciences Naturelles et Médicales, Bruxelles, nouvelle série, 22, 231 pp.

Liégeois, J.P., Black, R., 1987. Alkaline magmatism subsequent to collision in the Pan-African belt of the Adrar des Iforas (Mali). Geol. Soc. Spec. Publ. 30, 381–401.

Liégeois, J.P., Bertrand, J.M., Black, R., 1987. The subduction- and collision-related Pan-African composite batholith of the Adrar des Iforas (Mali): a review. Geol. J. 22, 185–211.

Liégeois, J.P., Sauvage, J.F., Black, R., 1991. The Permo-Jurassic alkaline province of Tadhak, Mali: geology, geochronology and tectonic significance. Lithos 27, 95–105.

Liégeois, J.P., Black, R., Navez, J., Latouche, L., 1994. Early and late Pan-African orogenies in the Aïr assembly of terranes (Tuareg shield, Niger). Precambr. Res. 67, 59–88.

Liégeois, J.P., Diombana, D., Black, R., 1996. The Tessalit ring complex (Adrar des Iforas, Malian Tuareg shield): a Pan-African, post-collisional, syn-shear, alkaline granite intrusion. In: Demaiffe, D. (Ed.), Petrology and Geochemistry of Magmatic Suite of Rocks in the Continental and Oceanic Crusts. ULB-MRAC, Bruxelles, pp. 227–244.

Liew, T.C., McCulloch, M.T., 1985. Genesis of granitoid batholiths of Peninsular Malaysia and implications for models of crustal evolution: evidence from a Nd–Sr isotopic and U–Pb zircon study. Geochim. Cosmochim. Acta 49, 587–600.

Martin, H., 1987. Archaean and modern granitoids as indicators of changes in geodynamic processes. Rev. Bras. Geosci. 17, 360–365.

McCulloch, M.T., Black, L.P., 1984. Sm–Nd isotopic systematics of Enderby Land granulites and evidence for the redistribution of Sm and Nd during metamorphism. Earth Planet. Sci. Lett. 71, 46–58.

Michard, A., Gurriet, P., Soudant, M., Albarède, F., 1985. Nd isotopes in French Phanerozoic shales: external vs. internal aspects of crustal evolution. Geochim. Cosmochim. Acta 49, 601–610.

Moreau, C., Rocci, G., Brown, W., Demaiffe, D., Perez, J.B., 1991. Paleozoic magmatism in the Aïr massif–Niger. In: Kampuzu, A.B., Lubala, T. (Eds.), Magmatism in Extensional Structural Settings. The Phanerozoic African Plate. Springer-Verlag, pp. 328–352.

Moreau, C., Demaiffe, D., Bellion, Y., Boullier, A.M., 1994. A tectonic model for the location of Paleozoic ring-complexes in Aïr (Niger, West Africa). Tectonophysics 234, 129–146.

Navez, J., 1995. Détermination d'éléments en traces dans les roches silicatées par ICP-MS. Rapport Annuel du Département de Géologie et Minéralogie 1993–1994, Musée Royal de l'Afrique Centrale, Tervuren, Belgique, pp. 139–147.

Nelson, B.K., De Paolo, D.J., 1985. Rapid production of continental crust 1.7 to 1.9 b.y. ago: Nd isotopic evidence from the basement of the North American mid-continent. Geol. Soc. Am. Bull. 96, 746–754.

Ouzegane, K., Boumaza, S., 1996. An example of ultrahigh-temperature metamorphism: orthopyroxene–sillimanite–garnet, sapphirine–quartz and spinel–quartz parageneses in Al–Mg granulites from In Hihaou, In Ouzzal, Hoggar. J. Metam. Geol. 14, 693–708.

Pearce, J.A., 1983. Role of the sub-continental lithosphere in magma genesis at active continental margins. In: Hawkesworth, C.J., Norry, M.J. (Eds.), Continental Basalts and Mantle Xenoliths. Shiva Publ., Nautwich, pp. 230–249.

Pearce, J.A., Albaster, T., Shelton, A.W., Searle, M.P., 1981. The Oman ophiolite as a Cretaceous arc-basin complex; evidence and implications. Philos. Trans. R. Soc. Lond., Ser. A 300, 299–317.

Pearce, J., Harris, N.B.W., Tindle, A.G., 1984. Trace element discrimination diagrams for the tectonic interpretation of granitic rocks. J. Petrol. 25, 956–983.

Peucat, J.J., Capdevila, R., Drareni, A., Choukroune, P., Fanning, C.M., Bernard-Griffiths, J., Fourcade, S., 1996. Major and trace element geochemistry and isotope (Sr, Nd, Pb, O) systematics of an Archaean basement involved in a 2.0 Ga very high-temperature (1000°C) metamorphic event: In Ouzzal massif, Hoggar, Algeria. J. Metam. Geol. 14, 667–692.

Rollinson, H., 1993. Using geochemical data: evaluation, presentation, interpretation. Longman, Harlow, 352 pp.

Shaw, D.M., 1968. A review of K–Rb fractionation trends by co-variance analysis. Geochim. Cosmochim. Acta 32, 573–601.

Steiger, R.H., Jäger, E., 1977. Subcommission on geochronology: convention on the use of decay constant in geo- and cosmochronology. Earth Planet. Sci. Lett. 36, 359–362.

Taylor, S.R., McLennan, S.M., 1985. The continental crust: its composition and evolution. Blackwell, Oxford, 312 pp.

Tuttle, O.F., Bowen, N.L., 1958. Origin of granites in the light of experimental studies in the system $NaAlSi_3O_8$–$KAlSi_3O_8$–SiO_2–H_2O. Mem. Geol. Soc. Am. 74, 153 pp.

Whalen, J.B., Currie, K.L., Chappell, B.W., 1987. A-type granites: geochemical characteristics, discrimination and petrogenesis. Contrib. Mineral. Petrol. 95, 407–419.

Williamson, J.H., 1968. Least square fitting of a straight line. Can. J. Phys. 46, 1845–1847.

Zindler, A., Hart, S.R., 1986. Chemical geodynamics. Annu. Rev. Earth Planet. Sci. 14, 493–571.